Journal of the Korean Physical Society, Vol. 72, No. 10, May 2018, pp. 1203∼1208

Effects of Electron Beam Irradiation and Thiol Molecule Treatment on the Properties of MoS_2 Field Effect Transistors

Barbara Yuri Choi, Kyungjune Cho, Jinsu Pak, Tae-Young Kim, Jae-Keun Kim, Jiwon Shin, Junseok Seo, Seungjun Chung and Takhee Lee*

Department of Physics and Astronomy, and Institute of Applied Physics, Seoul National University, Seoul 08826, Korea

(Received 7 December 2017)

We investigated the effects of the structural defects intentionally created by electron-beam irradiation with an energy of 30 keV on the electrical properties of monolayer MoS_2 field effect transistors (FETs). We observed that the created defects by electron beam irradiation on the MoS_2 surface working as trap sites deteriorated the carrier mobility and carrier concentration with increasing the subthreshold swing value and shifting the threshold voltage in MoS_2 FETs. The electrical properties of electron-beam irradiated MoS_2 FETs were slightly improved by treating the devices with thiol-terminated molecules which presumably passivated the structural defects of MoS_2. The results of this study may enhance the understanding of the electrical properties of MoS_2 FETs in terms of creating and passivating defect sites.

PACS numbers: 73.50.−h, 73.63.−b, 73.22.−f, 81.65.−b
Keywords: Molybdenum disulfide, Electron beam irradiation, Chemical treatment, Electrical properties
DOI: 10.3938/jkps.72.1203

I. INTRODUCTION

Two-dimensional transition-metal dichalcogenides (TMDCs), such as MoS_2, WS_2, $MoSe_2$, and WSe_2 have attracted significant attention due to their promising electrical and optical properties such as good electrical and optical properties, mechanical flexibility, and transparency [1–4]. In particular, TMDCs have tunable band gap energy, for example, the band gap of MoS_2 varies from indirect band gap of 1.2 eV to direct band gap of 1.9 eV as the number of MoS_2 layers changes from bulk to monolayer [5,6]. Furthermore, due to the direct band gap energy and excellent transparency of monolayer MoS_2 leading to strong photoluminescence, MoS_2 promises to be used for photosensor applications [7–15]. However, the advancement of MoS_2-based nanoelectronics is still limited by various types of defects such as point defects, dislocations, and grain boundaries on MoS_2 generated during the preparation process that are expected to affect the electrical and optical properties of MoS_2. Especially, the structural defects on MoS_2 can act as charge trap-sites in MoS_2 devices [16]. Because of this crucial importance of defects on the device properties, it is essential to characterize the defects on MoS_2 for realizing high performance MoS_2 device applications. In this regard, there have been many efforts to study the effect of the defects on the electrical and optical properties of MoS_2 by intentionally creating the structural defects, for example, by utilizing high-energy electron-beam (e-beam) irradiation [16], ions bombardment [17], or plasma treatments [18, 19]. For example, Parkin *et al.* reported that the channel current in MoS_2 field-effect transistors (FETs) decreased when the MoS_2 channels were exposed to 200 keV e-beam in a transmission electron microscope (TEM) system [16]. They observed that the current decreased as increasing the dose amount of irradiated electrons. This current reduction was explained by the structural defects, for example, mono-sulfur vacancies that were intentionally created by high-energy e-beam irradiation in TEM and acted as charge-trapping sites in MoS_2 channels. Similarly, Bertolazzi *et al.* exposed bombarded ion beams on MoS_2 channel and observed electrically degraded channel properties by intentionally created sulfur vacancies and defects [17]. Then, they treated the ion beam irradiated MoS_2 devices with hexanethiol ($CH_3(CH_2)_5SH$) molecules, and observed that the reduced current in the ion-irradiated MoS_2 devices was recovered to about 90% of the original current. They explained that this current recovery was because the thiol molecules could passivate the generated structural defects related to sulfur vacancies. Previously, our group also reported that the hexadecanethiol ($CH_3(CH_2)_{15}SH$) treatment on the pristine MoS_2 channel layer in FETs could decrease the current because the adsorbed thiol molecules passivated intrinsic sulfur vacancies which might act as electron donors

*E-mail: tlee@snu.ac.kr

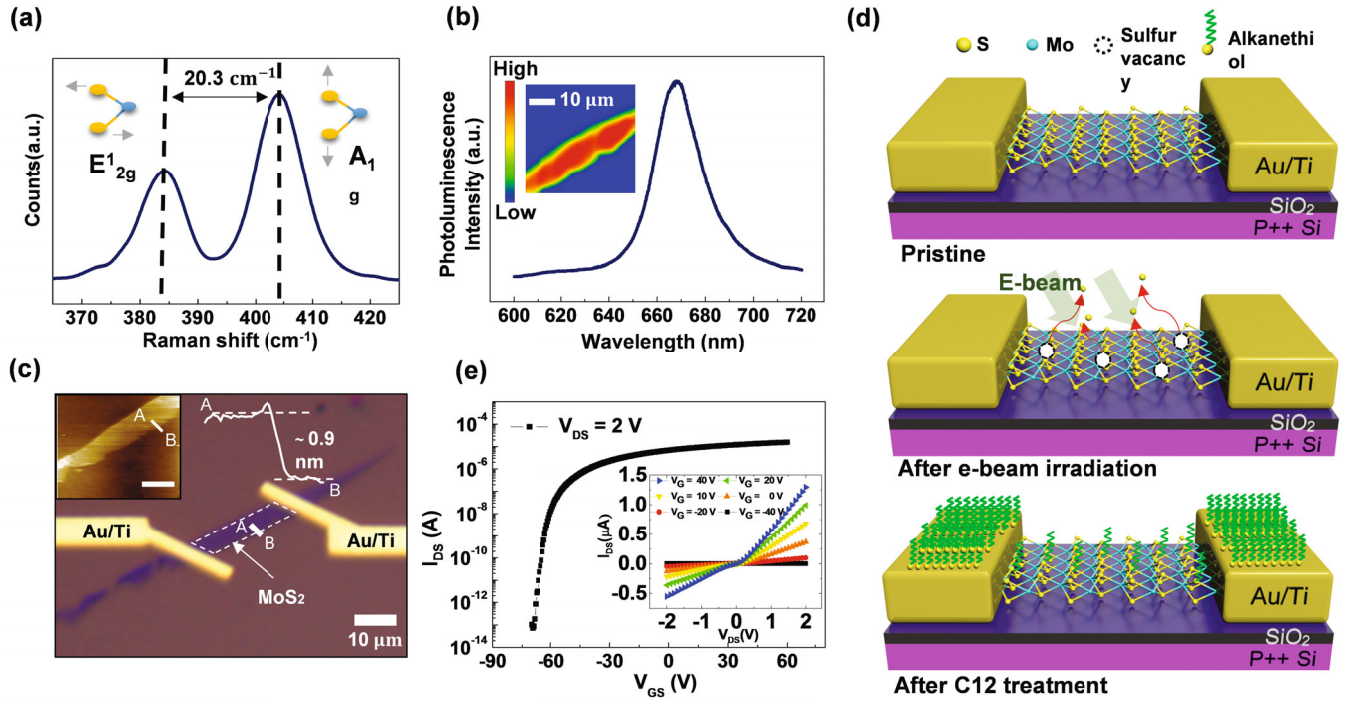

Fig. 1. (Color online) (a) Raman and (b) photoluminescence data of a monolayer MoS_2 flake. (c) Optical and AFM image of monolayer MoS_2 FET. Inset AFM graph shows that measured height of MoS_2 layer is $\sim$ 0.9 nm. (d) Schematic images of pristine, e-beam irradiated, and C12-treated MoS_2 FET. (e) I_{DS}-V_{GS} curve measured at a fixed V_{DS} = 2 V in a logarithmic scale. The inset shows I_{DS}-V_{DS} curves measured with V_{GS} varying from 40 to -40 V.

[20,21]. Although it is not thoroughly understood, the different behaviors of current changes (increase versus decrease) after the molecular treatment [21] might be associated with the different origins of the structural defects (intrinsic defects and intentionally created defects).

In this study, we investigated the effects of the structural defects intentionally created by a relatively low energy e-beam irradiation and thiol molecular treatment on the electrical properties of MoS_2 FETs. E-beam irradiation with 30 keV and dodecanethiol ($CH_3(CH_2)_{11}SH$) treatment were done to generate and passivate the structural defects in monolayer MoS_2, respectively. The created defects on the MoS_2 surface working as trap sites could deteriorate the carrier mobility and carrier concentration with increasing the subthreshold swing value and shifting the threshold voltage. Moreover, the degraded transport properties of e-beam irradiated MoS_2 FETs could be somewhat recovered by immersing them into dodecanethiol solutions which enabled chemical adsorption of thiol terminated molecules at the structural defects, for example, sulfur vacancy-related defect sites. To support these results, Raman and X-ray photoelectron spectroscopy (XPS) were conducted on the MoS_2 films.

II. EXPERIMENTS AND DISCUSSION

First, we transferred monolayer MoS_2 flakes with a mechanically exfoliating method using a scotch tape from a bulk MoS_2 crystal on 270 nm-thick SiO_2 grown on a heavily doped Si substrate to be used as a back gate in FETs. A Raman system (Nanobase, XperFam 200) and atomic force microscope (AFM) (Park Systems, NX10) were used to confirm that the transferred MoS_2 flakes were monolayer. The Raman system that we used had a laser excitation power of $\sim$ 0.5 mW, integration time of 2000 ms, and laser wavelength of 532 nm. We observed two active Raman modes of variation in MoS_2, *i.e.*, E^1_{2g} mode ($\sim$ 384.3 cm^{-1}) and A_{1g} mode (404.6 cm^{-1}), as shown in Fig. 1(a). Here, E^1_{2g} mode is the peak of in-plane vibrations of Mo atoms and S atoms in opposite direction, and A_{1g} mode is the peak of out of plane vibrations of S atoms in opposite direction. The difference value ($\sim$ 20.3 cm^{-1}) of A_{1g} and E^1_{2g} mode were observed, supporting that MoS_2 flakes were monolayer MoS_2 [22–24]. Also, a strong resonance peak at about 670 cm^{-1} region in the photoluminescence (PL) supports the monolayer MoS_2 (Fig. 1(b)).

Figure 1(c) shows the optical image of a fabricated MoS_2 FET and the inset image shows the AFM image of the prepared MoS_2 flake. A topographic cross-sectional profile along the line AB marked in the inset image is also shown in Fig. 1(c). The measured height of MoS_2

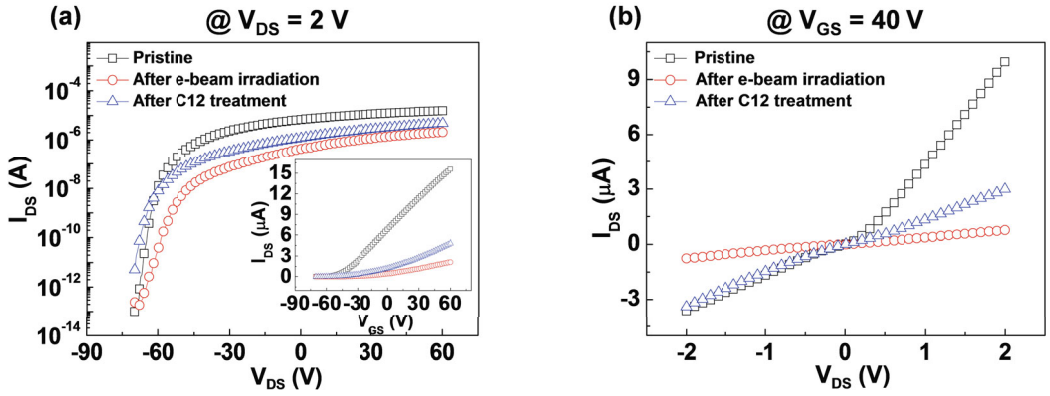

Fig. 2. (Color online) (a) I_{DS}-V_{GS} curves measured at a fixed V_{DS} = 2 V in a log scale for pristine, *e*-beam irradiated, and C12-treated MoS_2 FET. The inset shows I_{DS}-V_{GS} curve in the linear scale. (b) I_{DS}-V_{DS} curves measured at a fixed V_{GS} = 40 V for scale for pristine, *e*-beam irradiated, and C12-treated MoS_2 FET.

flake was found to be $\sim$ 0.9 nm which corresponds to monolayer MoS_2. To fabricate MoS_2 FETs, we defined the source and drain electrodes patterns on the transferred MoS_2 flake using an *e*-beam lithography system (JSM-6510, JEOL). Double-layer resist, *i.e.*, an electron resist polymer poly methyl methacrylate (PMMA) 950 K (5% concentration in anisole) and a buffer layer methyl methacrylate (MMA) (8.5%), MAA (9% concentration in ethyl lactate) were used for the patterning process. After developing the resists, Au (45 nm thick)/Ti (5 nm thick) layers were deposited as the source and drain electrodes using an *e*-beam evaporator (KVE-2004L, Korea Vacuum Tech.). Then, the fabrication of MoS_2 FETs were completed (top panel of Fig. 1(d)).

We characterized the electrical properties of the pristine MoS_2 FETs that were not treated with e-beams nor chemical treatments. Figure 1(e) shows the transfer curve (source-drain current *versus* gate voltage, I_{DS}-V_{GS}) of the pristine MoS_2 FET measured at a fixed source drain voltage (V_{DS} = 2 V), exhibiting typical n-type semiconducting behaviors. The inset of Fig. 1(e) shows the output curve (source-drain current *versus* source-drain voltage, I_{DS}-V_{DS}) of the device measured with gate voltages varying from 40 to -60 V. The electrical measurement were done in a vacuum ($\sim 10^{-3}$ Torr). The representative current on/off ratio and mobility of this MoS_2 FET (Fig. 1(e)) was found to be $\sim 10^8$ and $\sim$ 6.7 cm^2/Vs, respectively.

After the pristine MoS_2 FETs were characterized, we irradiated *e*-beam onto the MoS_2 devices using SEM, as schematically illustrated in the middle panel of Fig. 1(d). Note that we irradiated *e*-beam only the MoS_2 channel regions to avoid unwanted effects. The *e*-beam irradiation was performed under a high vacuum ($\sim 10^{-6}$ Torr) in the SEM chamber with an acceleration voltage of 30 kV and a dose of 1×10^5 μC/cm^2 condition. E-beam irradiation onto MoS_2 produces mostly mono-sulfur vacancies which act as defect sites [16]. After producing defects on MoS_2 by *e*-beam irradiation, we deposited dodecanethiol (denoted as C12) molecules onto the *e*-beam irradiated MoS_2 FETs (bottom panel of Fig. 1(d)) by placing the samples in dodecanethiol solution for 22 h in a N_2-filled glove box. The thiol (-SH) group of molecules tend to form a chemisorption bond with sulfur vacancy sites in MoS_2 [17]. Pristine, *e*-beam irradiated, and C12-treated MoS_2 channels were characterized with XPS (AXIS Supra) and Raman spectroscopy (XperRam 200, Nanobase Inc.). And, the electrical characteristics of pristine, *e*-beam irradiated, and C12-treated MoS_2 FETs were measured using a semiconductor parameter analyzer (Keithley, 4200-SCS) in a vacuum probe station (Janis, ST-500).

Figure 2(a) shows a series of transfer curves of a MoS_2 FET measured at a fixed V_{DS} = 2 V. The transfer curves were sequentially obtained for a pristine MoS_2 FET device, then after the same device was irradiated with *e*-beam, and then after C12 treatment. As shown in the figure, the source-drain current level dramatically decreased after *e*-beam irradiation process. This current reduction phenomenon could be explained by the defects created by *e*-beam irradiation process. After C12 treatment, the current level increased although it didn't fully recover to the original current level at the pristine condition. C12 molecules could passivate not only the intentionally generated defects by *e*-beam, but also the intrinsic sulfur vacancies which could behave as donor sites. After C12 treatment, some of the additional sulfur vacancies created by *e*-beam irradiation could be passivated via chemisorption of C12 molecules [17]. Therefore, the defect density in MoS_2 could be reduced after C12 treatment, which results in the current increase. At the same time, C12 molecules passivate the intrinsic sulfur vacancies which could behave as donor sites, which results in the current decrease. As a combined effects, the current of the MoS_2 FET increased slightly, but was not fully recovered after C12 treatment, as shown in Fig. 2(a). Figure 2(b) shows the output curves of pristine, *e*-beam irradiated, and C12 treated MoS_2 FET

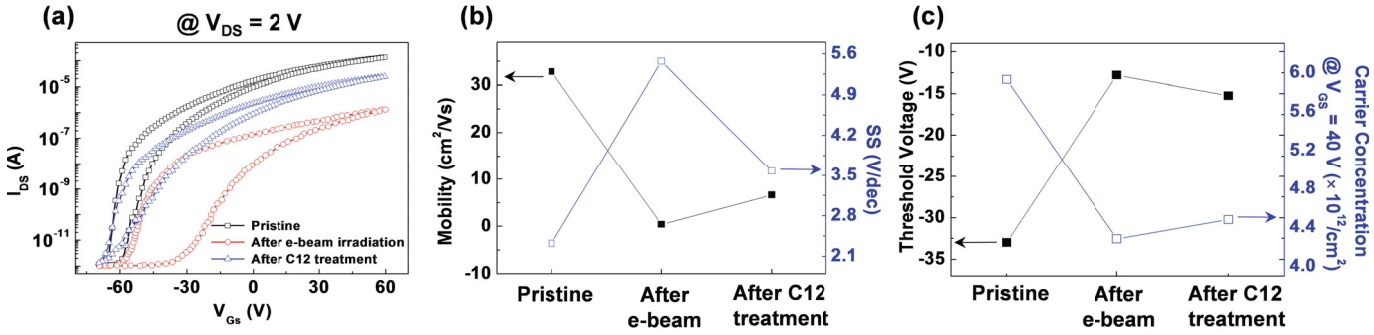

Fig. 3. (Color online) (a) Hysteresis of I_{DS}-V_{GS} curves in the log scale measured at a fixed $V_{DS} = 2$ V for pristine, e-beam irradiated, and C12-treated MoS_2 FET. (b) Mobility and SS value for pristine, e-beam irradiated, and C12-treated MoS_2 FET. (c) Threshold voltage and carrier concentration for pristine, e-beam irradiated, and C12-treated MoS_2 FET.

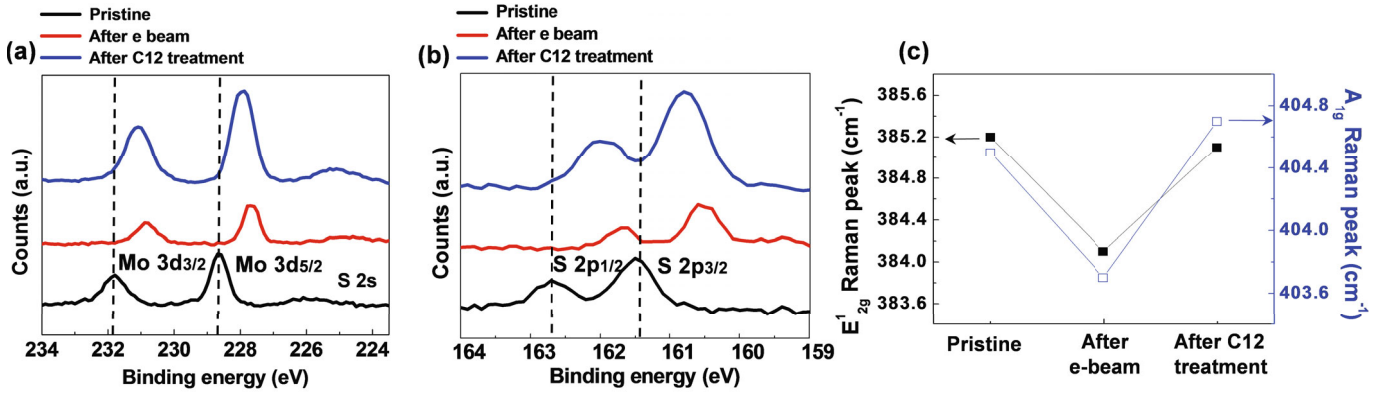

Fig. 4. (Color online) (a) XPS spectra of Mo 3d and (b) S 2p for pristine, e-beam irradiated, and C12-treated MoS_2. (c) Positions of the two Raman peaks for pristine, e-beam irradiated, and C12-treated MoS_2.

measured at the fixed V_{GS} of 40 V. Same tendency was observed in Fig. 2(b). We also observed similar behavior of the electrical properties with other devices (data not shown here).

Figure 3(a) shows the hysteresis in transfer characteristics of a MoS_2 FET for the three cases (pristine, after e-beam irradiation, and after C12 treatment). We investigated the hysteresis in I_{DS}-V_{GS} curves with a fixed source-drain voltage of 2 V. Each cyclic voltage, sweeping from $V_{GS} = -70$ V to 60 V and back to -70 V, was repeated for all the three cases in vacuum condition ($\sim 10^{-3}$ Torr). The magnitudes of the hysteresis window was extracted as the difference of the gate voltages in different sweeping directions at $I_{DS} = 1$ nA. The values of hysteresis window (ΔV) in the transfer curves of pristine, e-beam irradiated, and C12-treated MoS_2 FET were evaluated as ~ 13 V, 30 V, and 15 V, respectively. The hysteresis in the transfer curves could be affected by the charge trapping on the interface between MoS_2 and SiO_2 [25, 26]. The intentionally generated defects could act as charge-trapping sites, resulting in enlargement of the magnitude of hysteresis window [25]. Also, decrement in the magnitude of hysteresis window after C12 treatment could be explained by the reduction of induced defects by C12 molecules. Similarly, the current on/off ratio decreased after e-beam irradiation from $\sim 10^8$ to $\sim 10^6$, however it slightly increased after C12 treatment from $\sim 10^6$ to $\sim 10^7$.

The amount of defect sites is closely related to the carrier mobility and the subthreshold swing (SS) value of the FETs. Figure 3(b) shows mobility (black symbols) and SS (blue symbols) values estimated from the transfer curves for the three cases. The mobility values of the MoS_2 FETs were calculated by using the following formula: $\mu = \left(\frac{dI_{DS}}{dV_{GS}}\right) \times [L/WC_iV_{DS}]$, where L is the channel length (~ 2.4 μm), W is the channel width (~ 7.4 μm), V_{DS} is the source-drain voltage (2 V), and $C_i = (\varepsilon_0\varepsilon_r)/d \simeq 1.3 \times 10^{-4}$ F/m^2 is the capacitance between the MoS_2 channel and SiO_2 per area where ε_r is the relative permittivity of SiO_2 (~ 3.9), ε_0 is the permittivity of vacuum ($\sim 8.85 \times 10^{-12}$ F/m), and d is the thickness of the SiO_2 layer (270 nm). Note that the value of mobility substantially decreased from 32.8 cm^2/Vs to 0.4 cm^2/Vs, as shown in Fig. 3(b). The intentionally created defect sites degraded the mobility of MoS_2 FET after e-beam irradiation. On the other hand, the mobility slightly increased from 0.4 cm^2/V to 6.7 cm^2/Vs after the C12 treatment by passivating the defect sites. The SS value of the MoS_2 FET increased ($\Delta SS = 3.15$ V/dec)

after e-beam irradiation (Fig. 3(b)). Generally, the SS value of FET is proportional to the amount of defects. The increased amount of defects in MoS_2 channel by e-beam irradiation increased the SS value of the MoS_2 FET. Similar to the mobility, the SS value of the MoS_2 FET was improved (*i.e.*, decreased) after C12 treatment ($\Delta SS = 1.89$ V/dec).

Figure 3(c) show the threshold voltage (black symbols) and carrier concentration (blue symbols) for the MoS_2 FETs for the three cases. Here, the threshold voltage was estimated as the x-axis intercept of a linear fitting of the transfer curve. The threshold voltage of the MoS_2 FET shifted in the positive gate voltage direction after e-beam irradiation and returned in the negative gate bias direction after C12 treatment. And, the carrier concentration decreased after e-beam irradiation and slightly recovered after C12 treatment. Here, the carrier concentrations were estimated at a $V_{GS} = 40$ V with the formula: $n_e = Q/e = C_G|V_{GS} - V_{Th}|/e$, where C_G is the capacitance of the SiO_2 dielectric layer, V_{Th} is threshold voltage of the FET devices, and the e is the elementary charge.

To verify that the defects in MoS_2 channel were generated by e-beam irradiation and passivated by C12 molecular treatment, we conducted the XPS and Raman experiments. Figures 4(a) and 4(b) show the XPS data of pristine, e-beam irradiated, and C12-treated MoS_2 flakes. The atomic concentration of Mo and S for each case was evaluated from XPS data of each MoS_2 flake sample. The calculated concentration ratio between Mo and S slightly decreased after e-beam irradiation. Although 30 keV of irradiated e-beam has relatively low knock-on energy, it has enough ionization energy to create the structural defects such as sulfur vacancy-related defects. Therefore, the e-beam irradiation introduced additional defects with decreasing the ratio between Mo and S and decreased the source-drain current of MoS_2 FETs. After C12 treatment, C12 molecules passivated the structural defects and decreased the amount of defect sites. Therefore, the evaluated ratio between Mo and S and the current slightly recovered after C12 treatment. Also, we observed that the characteristic peak positions of MoS_2 shifted in low-energy direction after e-beam irradiation and slightly shifted back after C12 treatment due to their varied chemical environment, as shown in Figs. 4(a) and 4(b). Figure 4(c) summarizes the positions of two characteristic Raman active modes, E^1_{2g} and A_{1g}, of pristine, e-beam irradiated, and C12-treated MoS_2 flake. For pristine MoS_2 sample, the peak position of E^1_{2g} and A_{1g} mode was 385.2 cm^{-1} and 404.5 cm^{-1}, respectively. The peak difference of two active modes was calculated as 19.3 cm^{-1}, which corresponds to monolayer MoS_2 [27,28]. As shown in Fig. 4(c), both modes of MoS_2 flake were red shifted after e-beam irradiation and shifted back to high energies after C12 treatment.

III. CONCLUSION

In summary, we investigated the effects of electron beam irradiation and thiol molecular treatment on MoS_2 FETs. The structural defects generated by electron beam irradiation acted as charge trap sites, so that they degraded the electrical properties of MoS_2 FETs in terms of current level, mobility, and subthreshold swing. And, thiol molecular treatment somewhat recovered the degraded electrical properties of MoS_2 FETs by passivating the structural defects. This study may enhance the understanding of the defects intentionally generated by energetic particles and the molecular passivation of those defects on the electrical properties of MoS_2 related nanoelectronic devices.

ACKNOWLEDGMENTS

The authors appreciate the financial support of the National Creative Research Laboratory program (Grant No. 2012026372) through the National Research Foundation of Korea, funded by the Korean Ministry of Science and ICT.

REFERENCES

[1] Q. H. Wang, K. Kalantar-Zadeh, A. Kis, J. N. Coleman and M. S. Strano, Nat. Nanotechnol. **7**, 699 (2012).
[2] B. Radisavljevic, A. Radenovic, J. Brivio, V. Glacometti and A. Kis, Nat. Nanotechol. **6**, 147 (2011).
[3] H. Fang, S. Chuang, T. C. Chang, K. Takei, T. Takahashi and A. Javey, Nano Lett. **12**, 3788-2792 (2012).
[4] D, Jariwala, V. K. Sangwan, L. J. Lauhon, T. J. Marks and M. C. Hersam, ACS Nano **8**, 1102 (2014).
[5] K. Kam and B. Parkinson, J. Phys. Chem. **86**, 463 (1982).
[6] K. F. Mak, C. Lee, J. Hone, J. Shan and T. F. Heinz, Phys. Rev. Lett. **105**, 136805 (2010).
[7] K. Novoselov, A. K. Geim, S. Morozov, D. Jiang, Y. Zhang, S. Dobonos, I. Grigorieva and A. Firsov, Science **306**, 666 (2004).
[8] K. S. Novoselov, D. Jiang, F. Schedin, T. J. Booth, V. V. Khotkevich, S. V. Morozoc and A. K. Geim, **102**, 10451 (2005).
[9] A. Kuc, N. Zibouche and T. Heine, Phys. Rev. B: Condens. Matter Mater. Phys. **83**, 245213 (2013).
[10] Y. L. Hyang, Y. F. Chen, W. J. Zhang, S. Y. Quek, C. H. Chen, L. J. Li, W. T. Hsu, W. H. Chang, Y. J. Zheng and W. Chen, Nat. Commun. **6**, 6298 (2015).
[11] J. D. Lin, C. Han, F. Wang, R. Wang, D. Xiang, S. Q. Qin, X. Zhang, A. X, L. Wang, H. Zhang and A. T. S. Wee, ACS Nano **8**, 5323 (2014).
[12] S. Wi, H. Kim, H. Nam, L. J. Guo, E. Meyhofer and X. G. Liang, ACS Nano **8**, 5270 (2014).
[13] R. Cheng, S. Jiang, Y. Chen, Y. Liu, N. Weiss, H. C. Cheng, H. Wu, Y. Huang and X. F. Duan, Nat. Commun. **5**, 5143 (2014).

[14] X. G. Liang, ACS Nano **7**, 5870 (2013).
[15] O. Lopez-Sanchez, D. Lembke, M. Kayci, A. Radenovic and A. Kis, Nat. Nanotechnol. **8**, 497 (2013).
[16] W. M. Parkin *et al.*, ACS Nano. **10**, 4134 (2016).
[17] S. Bertolazzi, S. Bonacchi, G. Nan, A. Pershin, D. Beljonne and P. Samori, Adv. Mater. **29**, 1606760 (2017).
[18] H. Li *et al.*, Nat. Mater. **15**, 48 (2015).
[19] B. Peng, G. Yu, Y. Zhao, Q. Xu, G. Xing, X, Liu, D. Fu, B. Liu, J. R. S. Tan, W. Tang, H. Lu, J. Xie, L. Deng, T. C. Sum and K. P. Loh, ACS Nano **10**, 6383 (2016).
[20] H. Qiu, T. Xu, Z. Wang, W. Ren, H, Nan, Z, Ni, Q, Chen, S. Yuan, F. Miao, F. Song, G. Long, Y. Shi, L. Sun, J. Wang and X. Wang, Nat. Commun. **4**, 2642 (2013).
[21] K. Cho, M. Min, T. Y. Kim, H. Jeong, J. Pak, J. K. Kim, J. Jang, S. J. Yun, Y. H. Lee, W. K. Hong and T. K. Lee, ACS Nano **9**, 8044 (2015).
[22] L. Liang and V. Meunier, Nanoscale **6**, 5394 (2014).
[23] C. Lee, H. Yan, L. E. Brus, T. F. Heinz, J. Hone and S. Ryu, ACS Nano **4**, 2695 (2010).
[24] H. Li, Q. Zhang, C. C. R. Yap, B. K. Tay, T. H. T. Edwin, A. Olivier and D. Baillargeat, Adv. Funct. Mater. **22**, 1385 (2012).
[25] Y. Y. Illarionov, G. Rzepa, M. Waltl, T. Knobloch, A. Grill, M. M. Furchi, T. Mueller and T. Grasser, 2D Mater. **3**, 035004 (2016).
[26] A. D. Bartolomeo, L. Genovese, F. Giubileo, L. Lemmo, G. Luong, T. Foller and M. Schleberger, 2D Mater. **5**, 015014 (2017).
[27] M. A. Baker, C. Lenardi and W. Gissler, Appl. Surf. Sci. **150**, 255 (1999).
[28] P. A. Spevack and N. S. McIntyr, J. Phys. Chem. **97**, 1103 (1993).